Siehe auch: Theoretical and Applied Fracture Mechanics, Volume 90, 2017, S. 122-132, https://doi.org/10.1016/j.tafmec.2017.03.013
Preprint

Numerical crack path prediction under mixed-mode loading in 1D quasicrystals

Zhibin Wang[a,*], Andreas Ricoeur[a]

[a] *Institute of Mechanics, Department of Mechanical Engineering, University of Kassel, Mönchebergstraße 7, 34125 Kassel, Germany*

Abstract

Quasicrystals are being implemented in industry since this new class of materials appears to have some peculiar properties. However, the fracture behaviour of quasicrystals is not yet clear, which could be a hindrance to its wide usage. This work adopts the generalized linear elastic framework of fracture theory in quasicrystals and develops numerical tools in a finite element environment to compute the fracture quantities. Crack growth is simulated in diverse specimens undergoing an intrinsic mixed-mode loading and the influence of the phonon-phason coupling effect on crack paths is investigated.

Keywords: quasicrystal, crack path prediction, numerical simulation, phonon-phason coupling, finite elements

1. Introduction

Quasicrystals, abbreviated as QCs, are a new class of materials and have been widely acknowledged for about 3 decades [1]. The QCs have special atomic or molecular structure, neither like crystals which have the rigorous periodic atomic arrangement and the symmetric point group, nor like amorphous solids where the atoms are totally disordered. In diffraction patterns of QCs, sharp peaks can be found and they exhibit 5-, 10-, 12-fold or some other orientational symmetries, which are disallowed for classic crystals. It denotes that the QCs have long-range orientational order but no translational symmetry. The distribution of atoms is quasiperiodic rather

*Corresponding author
Email address: zhibin.wang@uni-kassel.de (Zhibin Wang)

than periodic and in short order, however, the structure still has crystalline features, so it was named as quasicrystal [2].

Depending on in how many directions the atom arrangement is quasiperiodic, QCs can be categorized into three sub-classes, i.e. 1D, 2D and 3D [3]. The sequence of the atoms in a quasiperiodic direction, normally consisting of two different intervals, is not ordered randomly. In fact, it follows certain mathematical rules, for details see [4]. In other words, the sequences of the arrangements are the consequence of equilibrium of the thermodynamic potential. Loading a QC structure mechanically, the quasiperiodic arrangement is influenced going along with atomic flips, denoted as phason displacements, which are introduced as a new degree of freedom. For the conventional degree of freedom, the denomination phonon displacement is borrowed from incommensurate crystals [5] describing the changes of position of atoms. The reason for this nomenclature is that the elastic displacement in condensed matter is treated like sound wave propagation, thus speaking of phonon excitation.

Since the phonon and phason degrees of freedom both affect the free energy acting mutually, the mechanical problems of quasicrystals are often investigated within the framework of coupled problems [6, 7]. In terms of geometrical crystallography, due to the periodicity of the structure crystals are mathematically represented by three unit vectors $\vec{e}_i$. However, the QCs with aperiodic arrangement need more than three unit vectors to be mathematically expressed, where the additional unit vectors indicate the structural sequence. Hence, the basic three unit vectors span a physical or phonon space $\mathrm{E}^{\parallel}$. The space constructed by the additional unit vectors is complemented to the physical space, so it is termed as complementary or mathematical space with a perpendicular symbol $\mathrm{E}^{\perp}$ [8], being attributed to the phason fields. The displacement degrees of freedom are accordingly denoted as $u_i^{\parallel}$ and $u_i^{\perp}$. The total displacement is related to the physical and complementary unit vectors as

$$\begin{pmatrix} u_i^{\parallel} \\ u_i^{\perp} \end{pmatrix} = \begin{pmatrix} u_i \\ W_i \end{pmatrix} = u_i \vec{e}_i^{\,\parallel} + W_i \vec{e}_i^{\,\perp}, \tag{1}$$

where summation $i = 1, 2, 3$ over repeated indices is implied. Eq. (1) represents the general case of a 3D QC. For a 1D QC there is just one complementary unit vector, i.e. $\vec{e}_i^{\,\perp} = \vec{e}_1^{\,\perp}$.

The physical properties of QCs are investigated massively, like thermodynamics, light propagation, electron transport, magnetism, conduction, elasticity, dislocation mechanisms and so on [9, 10, 11, 12, 13]. The progress

of these investigations extends essentially the fields of application of QCs, for instance, wear resistant coating, hydrogen storage or sintering powders for rapid prototyping [14].

Many papers have been published, dealing with diverse problems of the extended theory of elasticity for QCs. Various boundary value problems have been investigated applying different methods, providing solutions for e.g. inclusions [15, 16], interfaces [17] or Green's functions [18, 19]. Some papers address crack problems in QCs giving solutions in the structure or in the crack tip near field and providing fracture mechanical loading quantities [20, 21]. Finite element (FE) approaches of QCs including cracks have been established in [22, 23]. A meshless local Petrov-Galerkin approach is applied to dynamic crack problems in QCs in [24]. The problem of crack growth in QCs has been treated on the nanoscale by a molecular dynamics approach [25]. Crack deflection in QCs is handled within a continuum mechanical framework [26], where different crack tip loading quantities, i.e. J-integral, energy release rate and stress intensity factors are related to each other and exploited with respect to crack deflection criteria.

The focus of this work is on macroscopic cracks in 1D quasicrystalline plates. The generalized elastic framework and the fracture theory of QCs are briefly given in the first two sections. Based on a variational principle and the constitutive equations, the weak formulation of QCs is derived and applied in a FE context in the next section, where the constitutive behaviour is implemented in special USER elements. Then, two numerical approaches for computing fracture mechanical loading quantities in a post processing are introduced. In the results section, different numerical models with crack paths are presented. The crack growth is simulated applying an adaptive re-meshing algorithm and the J-integral criterion is adopted to determine the direction of crack growth under mixed-mode loading.

2. The linear elasticity of 1D quasicrystals

The phonon strain ϵ_{ij} is defined as in conventional theory of elasticity. However, the phason displacement vector W_i is a function of phonon coordinates only, i.e. $W_i(x_i^{\parallel})$, and the phason strain w_{ij} isn't symmetric by nature:

$$\epsilon_{ij} = \frac{1}{2}(u_{i,j} + u_{j,i}), \quad w_{ij} = W_{i,j} \neq W_{j,i}. \tag{2}$$

It is important to note that the first index in W_{ij} is allocated to the complementary space, while the second one, stemming from a spacial derivative, is attributed to the physical space.

The elastic free energy of a QC is given as a function of the phonon strain and the phason strain [7]. The free energy density can be expanded into the Taylor series, for infinitesimal displacement neglecting higher order terms. As usual in linear elasticity, the quadratic terms remain:

$$\begin{aligned}\Phi &= \Phi_{uu} + \Phi_{ww} + \Phi_{uw} \\ &= \frac{1}{2}C_{ijkl}\epsilon_{ij}\epsilon_{kl} + \frac{1}{2}K_{ijkl}w_{ij}w_{kl} + R_{ijkl}\epsilon_{ij}w_{kl},\end{aligned} \tag{3}$$

where Φ_{uu}, Φ_{ww} and Φ_{uw} are the specific energies of pure phonon, pure phason and phonon-phason coupling, respectively. C_{ijkl} is the phonon elastic stiffness tensor, K_{ijkl} is the stiffness tensor in the phason field and R_{ijkl} denotes the phonon-phason coupling tensor. Furthermore, the stiffness and coupling tensors can be expressed by means of partial derivatives, i.e.

$$\begin{aligned} C_{ijkl} &= \frac{\partial^2\Phi}{\partial\epsilon_{ij}\partial\epsilon_{kl}}, \qquad C_{ijkl} = C_{klij} = C_{ijlk} = C_{jikl}, \\ K_{ijkl} &= \frac{\partial^2\Phi}{\partial w_{ij}\partial w_{kl}}, \qquad K_{ijkl} = K_{klij}, \\ R_{ijkl} &= \frac{\partial^2\Phi}{\partial\epsilon_{ij}\partial w_{kl}}, \qquad R_{ijkl} = R_{jikl}. \end{aligned} \tag{4}$$

Eqs. (4) comprise all symmetry conditions of the constitutive tensors. In particular, since the symmetry property is absent in the phason strain, K_{ijkl} and R_{ijkl} exhibit just one symmetric property each, where the first two indices of the coupling tensor are always attributed to the phonon and the last two to the phason fields. The Betti theorem of reciprocity is thus not valid at that point.

From Eqs. (3) and (4) the governing constitutive equations of quasicrystals are derived as

$$\begin{aligned}\sigma_{ij} &= \frac{\partial\Phi}{\partial\epsilon_{ij}} = C_{ijkl}\epsilon_{kl} + R_{ijkl}w_{kl}, \\ H_{ij} &= \frac{\partial\Phi}{\partial w_{ij}} = R_{klij}\epsilon_{kl} + K_{ijkl}w_{kl}.\end{aligned} \tag{5}$$

Similar to the phonon stress σ_{ij} and the traction $t_i = \sigma_{ji}n_j = \sigma_{ij}n_j$, the corresponding phason terms H_{ij} and $h_i = H_{ij}n_j$ are introduced [7]. Especially, the index i of the phason stresses H_{ij} and h_i is attributed to the complementary space, while the index j represents geometrical quantities, corresponding to the respective indices of the phason strain. Just as phason strain, phason stress thus lacks symmetry. Since the phason stress and

traction don't have a physical interpretation within a classical mechanical sense, a boundary value problem can only be formulated in terms of pure phonon loading.

Due to the restricted symmetry of the coupling tensor R_{ijkl} according to Eq. (4), the Maxwell relation is not satisfied, i.e.

$$\frac{\partial \sigma_{ij}}{\partial w_{kl}} \neq \frac{\partial H_{ij}}{\partial \epsilon_{kl}}. \tag{6}$$

In the following, a compact Voigt notation for second and fourth order tensors is introduced, e.g. σ_{Ij}, where the lowercase index runs as usual from 1 to 3 for conventional spatial elastic fields and the uppercase index is extended to 6 for general 3D QCs consisting of phonon and phason variables:

$$\sigma_{Ij} = (\sigma_{1j}, \sigma_{2j}, \sigma_{3j}, H_{1j}, H_{2j}, H_{3j})^{\mathrm{T}}. \tag{7}$$

For the special case of 1D QCs in a plane problem, $i, j, k, l = 1$ or 2, and $I, K = 1$ to 3, where $I, K = 3$ denotes the phason variable. Also in this way, the stiffness and coupling tensors can be compressed as follows

$$C_{IjKl} = \begin{cases} C_{ijkl} & \text{if } 1 \leq I, K \leq 2 \\ K_{1j1l} & \text{if } I, K = 3 \\ R_{ij1l} & \text{if } I = 3 \text{ or } K = 3 \end{cases}. \tag{8}$$

3. Linear Elastic Fracture mechanics of QCs

3.1. Fracture quantities in 1D QCs

Considering a 1D QC plate with a crack within the framework of linear elasticity of QCs, the phonon and the phason stresses exhibit the same type of singularity at the crack tip [27] and the stress intensity factors (SIFs) can be generalized as follows

$$K_P = (K_{II}^{\parallel}, K_I^{\parallel}, K^{\perp})^{\mathrm{T}}. \tag{9}$$

The first two are phonon stress intensity factors which are associated with shear and tensile modes, respectively, the last one is the phason SIF. Since there is only one SIF from the phason field for 1D QCs, thus lacking different crack opening modes, the phason SIF is identified just by a perpendicular symbol. Based on linear elasticity of QCs and generalized SIFs, Gao et al.

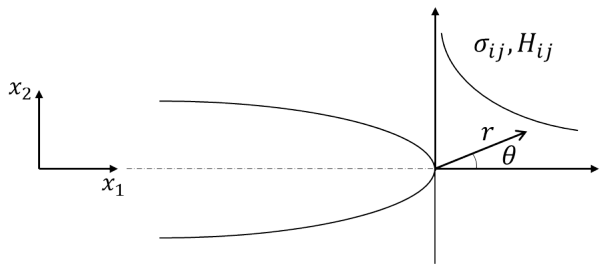

Figure 1: Polar coordinates (r, θ) in the vicinity of an opened crack tip and the stresses σ_{ij}, H_{ij} on the ligament.

[28] have derived the general near-tip field solutions

$$\begin{aligned}
\sigma_{I1}(r,\theta) &= -\frac{1}{\sqrt{2\pi r}}\Re\{B_{IN}\, P^{\mathrm{S1}}_{NM}\, B^{-1}_{MJ}\}K_J,\\
\sigma_{I2}(r,\theta) &= \frac{1}{\sqrt{2\pi r}}\Re\{B_{IN}\, P^{\mathrm{S2}}_{NM}\, B^{-1}_{MJ}\}K_J,\\
u_I(r,\theta) &= \sqrt{\frac{2r}{\pi}}\Re\{A_{IN}\, P^{\mathrm{u}}_{NM}\, B^{-1}_{MJ}\}K_J,
\end{aligned} \tag{10}$$

in a local crack tip coordinate system, see Fig. 1. The matrices A_{IN}, B_{IN} and P_{NM} are characteristic matrices depending on the material constants solely. P_{NM} are diagonal matrices in which the coefficients are functions of θ and eigenvalues p_N, see Appendix A.

The well-known energy release rate G is defined as the total potential energy per unit surface reduced during crack propagation

$$G = \lim_{\Delta A \to 0} \frac{-\Delta\Pi}{\Delta A} = -\frac{d\Pi}{dA}, \tag{11}$$

where $\Delta\Pi = -\Delta W^s$ is the reduced total potential energy of the system being equal to the negative work which is required for crack closure, in case of a reversal of the quasi-static process of crack growth [29].

This reversal procedure is implemented mathematically as crack closure integral, where the energy release rate is introduced as the work required for closing a crack incrementally in a range where the analytical near-tip solutions are valid. Besides the classical energy release rate G, an independent quantity H can be derived from a slightly modified crack closure integral [30, 31]. While the former is associated with the stress components σ_{i2} and H_{i2}, the latter is going along with σ_{i1} and H_{i1}. Substituting Eqs.

(10) into the respective integrals finally yields

$$\begin{aligned} G &= \frac{1}{2} K_P Y_{PQ} K_Q, \\ H &= -\frac{1}{2} K_P S_{PJ} Y_{JQ} K_Q, \end{aligned} \tag{12}$$

where

$$Y_{PQ} = \Re\{i A_{PN} B_{NQ}^{-1}\} \tag{13}$$

is the generalized Irwin matrix for QCs and

$$S_{PJ} = \Re\{B_{PN}^{-1} P_{NM}^{\mathrm{S1}}(\theta = 0) B_{MJ}\}. \tag{14}$$

Whereas a unique physical meaning is attributed to the energy release rate G, an interpretation of H with respect to crack closure is not known. The second energy rate is rather an auxiliary quantity, which may be useful e.g. in numerical fracture analysis [31], in particular in connection with the J-integral [26].

The path independent J-integral is another important fracture quantity, reading as follows

$$J_k = \oint_\Gamma Q_{kj} n_j \, \mathrm{d}\Gamma, \tag{15}$$

where

$$Q_{kj} = \Phi \delta_{kj} - \sigma_{ij} u_{i,k} - H_{ij} W_{i,k} \tag{16}$$

is the generalized energy-momentum or Eshelby tensor [32, 23, 26]. Generally,

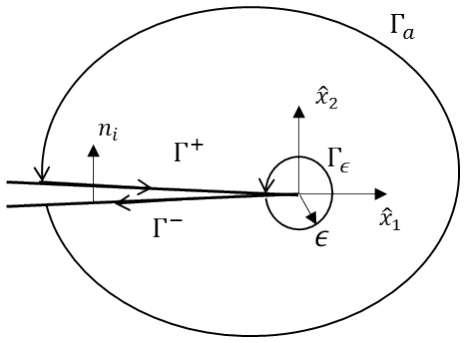

Figure 2: Contours of the J-integral; arrows indicate the orientations of the integration paths.

according to Fig. 2, a closed contour can be constructed including both crack

surfaces, however, excluding the crack tip. Thus, without any heterogeneity or defect in the enclosed domain the J-integral vanishes:

$$J_k = \oint_{\Gamma} Q_{kj} n_j \, \mathrm{d}\Gamma = \oint_{\Gamma_a + \Gamma^+ - \Gamma_\epsilon + \Gamma^-} Q_{kj} n_j \, \mathrm{d}\Gamma = 0. \tag{17}$$

Nevertheless, as long as the inner contour Γ_ϵ is sufficiently small, the J-integral can be calculated only based on Γ_ϵ. From Eq. (17) the J-integral is obtained as

$$\begin{aligned} J_k &= \lim_{\epsilon \to 0} \int_{\Gamma_\epsilon} Q_{kj} n_j \, \mathrm{d}\Gamma \\ &= \int_{\Gamma_a} Q_{kj} n_j \, \mathrm{d}\Gamma + \lim_{\epsilon \to 0} \int_{\Gamma^+ + \Gamma^-} (\Phi n_k - t_i u_{i,k} - h_i W_{i,k}) \, \mathrm{d}\Gamma. \end{aligned} \tag{18}$$

The crack surface integral requires some discussion. The phason tractions not being physical have to vanish at the crack faces, i.e. $h_i = 0$. If the phonon tractions are also zero and a straight crack is assumed with a crack tip coordinate system $(\hat{x}_1, \hat{x}_2)$ as indicated in Fig. 2, the calculation of J_1 does not require an integration along Γ^+ or Γ^- and Γ_a can be chosen arbitrarily. For the more general case of curved unloaded crack faces, the J-integral in Eq. (18) is reduced to

$$J_k = \int_{\Gamma_a} Q_{kj} n_j \mathrm{d}\Gamma + \lim_{\epsilon \to 0} \int_{\Gamma^+ + \Gamma^-} \Phi n_k \mathrm{d}\Gamma, \tag{19}$$

where the potential Φ according to Eq. (3) is vastly diminished due to stress and continuity conditions at the crack faces. The accurate calculation of the crack face integral requires special numerical treatment [33].

If the local orthogonal coordinate system $(\hat{x}_1, \hat{x}_2)$ is located in a way as it is shown in Fig. 2, and the unit vector of crack growth direction z_k is in the $\hat{x}_1$-axis, the relation of the energy release rate and the J_k-vector $G = J_k z_k$ yields the first of the following equations:

$$G = J_1, \qquad H = -J_2. \tag{20}$$

The latter relation is known from classical elasticity [30]. That it also holds for QCs can be shown analytically from Eqs. (12) and (18) applying the near-tip solutions according to Eq. (10). With Eqs. (12) and (20) the J_k-vector can thus be calculated from SIFs.

3.2. Crack deflection criterion for QCs at mixed-mode loading

If in conventional mechanics only the simple tensile mode is considered due to symmetrical loading and geometry, the crack grows straightforward along its ligament. Under mixed-mode loading, in a sense of unsymmetrical loading and the restriction $K_I \gg K_{II}$, the J-integral criterion has been proven to be appropriate and is adopted here to predict the crack growth deflection. It postulates that the crack extends along the direction of the crack tip configurational force, see Fig. 3. According to $G = J_k z_k$, the scalar product $J_k z_k$ is maximal if z_k and J_k are linearly dependent, thus leading to a maximum of the energy release rate. The deflection angle is accordingly determined as

$$\bar{\theta} = \arctan\left(\frac{J_2}{J_1}\right) = \arctan\left(\frac{-H}{G}\right) = \arctan\left(\frac{K_P S_{PJ} Y_{JQ} K_Q}{K_P Y_{PQ} K_Q}\right). \qquad (21)$$

The angle can be computed either directly from the path-independent J-integral applying Eq. (18) or (19), respectively, from the crack closure integral or alternatively from otherwise determined SIFs, see Eq. (12).

Finally, it should be noted that in QCs there is an intrinsic mixed-mode loading due to the phonon-phason coupling, where during crack growth $K^{\perp}$ is small compared to $K_I^{\parallel}$, just as $K_{II}^{\parallel}$. The J-integral criterion being thermodynamically motivated introduces crack growth as a process of global energy minimization, where phonon and phason energies are equally taken into account.

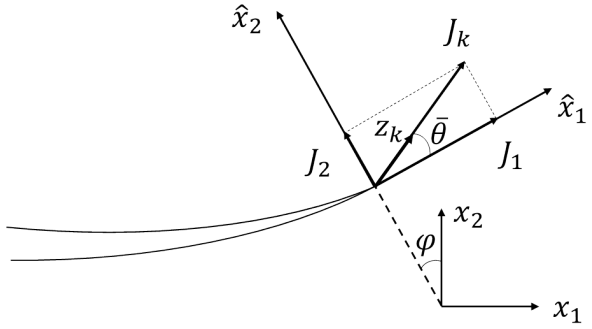

Figure 3: J-integral criterion for the crack deflection angle $\bar{\theta}$ and local crack tip as well as global coordinate systems.

3.3. Crack deflection and transformation of material related matrices

The selected 1D QC in this work shows transversely isotropic properties, with the quasicrystalline axis (QA) being perpendicular to an isotropic

crystalline plane. The QA is always in the x_1-x_2-plane and thus perpendicular to the crack front. The characteristic matrices and the Irwin matrix in Eqs. (10) and (12) refer to a local crack tip coordinate system $(\hat{x}_1, \hat{x}_2)$, see Fig 3, only depending on the material constants. The characteristic matrices and Irwin matrix therefore change due to crack deflection since the local coordinate system rotates with respect to the material axes which are aligned with the global coordinate system (x_1, x_2). A transformation is not straightforward, however, since e.g. Y_{PQ}, in fact being represented by a 3×3-matrix for plane problems in 1D QCs, is not a 2$^{\text{nd}}$ order tensor in a strict mathematical sense.

The transformation rules for these matrices are being derived in the following, starting from the Stroh formalism, which is briefly outlined in Appendix B. A similar approach is found in [34] which is, however, just available in Chinese, and has been modified here for the sake of more clarity. Some results in terms of Eqs. (31) and (36) are found in [35]. The final result has been verified numerically in this work.

First, a transformation matrix has to be introduced, accounting for two geometrical dimensions $\vec{e}_1^{\,\parallel}$ and $\vec{e}_2^{\,\parallel}$ in the physical space as well as one dimension $\vec{e}^{\,\perp}$ of the complementary space, i.e.

$$\vec{e}_I = (\vec{e}_1^{\,\parallel}, \vec{e}_2^{\,\parallel}, \vec{e}^{\,\perp})^{\mathrm{T}}. \tag{22}$$

The transformation matrix is thus defined as

$$\begin{aligned} \Omega_{IJ} = \hat{\vec{e}}_I \cdot \vec{e}_J &= |\hat{\vec{e}}_I||\vec{e}_J| \cos(\hat{\vec{e}}_I, \vec{e}_J) \\ &= \begin{pmatrix} \cos\varphi & \sin\varphi & 0 \\ -\sin\varphi & \cos\varphi & 0 \\ 0 & 0 & 1 \end{pmatrix}, \end{aligned} \tag{23}$$

where φ is the angle between the local coordinate system $\hat{x}_i$ and the global one x_i, see Fig. 3. A scalar product of physical and complementary basic vectors $\vec{e}_i^{\,\parallel}$ and $\vec{e}^{\,\perp}$ doesn't make sense, thus the respective coordinates of the 3×3-matrix in Eq. (23) are zero. A second transformation matrix is introduced just for the rotation in the plane physical space:

$$\Omega_{ij} = \begin{pmatrix} \cos\varphi & \sin\varphi \\ -\sin\varphi & \cos\varphi \end{pmatrix}. \tag{24}$$

The generalized stress and elastic tensors are transformed in the familiar

way

$$\hat{\sigma}_{Ij} = \Omega_{IM}\Omega_{jn}\sigma_{Mn}, \tag{25}$$

$$\hat{C}_{IjKl} = \Omega_{IM}\Omega_{jn}\Omega_{KP}\Omega_{lq}C_{MnPq}. \tag{26}$$

C_{MnPq} is the compressed stiffness tensor defined in Eq. (8). Furthermore, according to Eq. (B.3) an ansatz for the displacements reads

$$\hat{u}_I = \hat{a}_I \hat{f}(\hat{z}) \qquad \hat{z} = \hat{x}_1 + \hat{p}\hat{x}_2. \tag{27}$$

With the transformation matrix Ω_{ij}, $\hat{z}$ can be expanded as a function of x_i and φ:

$$\hat{z} = (\cos\varphi\, x_1 + \sin\varphi\, x_2) + \hat{p}(-\sin\varphi\, x_1 + \cos\varphi\, x_2). \tag{28}$$

The local displacement is likewise transformed from the global displacement as

$$\hat{u}_I = \Omega_{IJ}u_J = \Omega_{IJ}\, a_J f(z). \tag{29}$$

Since $\hat{u}_I$ depends on both z and $\hat{z}$, Eqs. (29) and (27), and $\hat{f}$ as well as f are arbitrary functions, $\hat{z}$ has to be a function of $z = x_1 + px_2$ as well [35]. Assorting x_i in Eq. (28) yields

$$\hat{z} = (\cos\varphi - \hat{p}\sin\varphi)(x_1 + \frac{\sin\varphi + \hat{p}\cos\varphi}{\cos\varphi - \hat{p}\sin\varphi}\, x_2). \tag{30}$$

So the relations of p and $\hat{p}$ are obtained as

$$p = \frac{\sin\varphi + \hat{p}\cos\varphi}{\cos\varphi - \hat{p}\sin\varphi} \tag{31}$$

or

$$\hat{p} = \frac{p\cos\varphi - \sin\varphi}{p\sin\varphi + \cos\varphi}. \tag{32}$$

Inserting Eq. (31) into Eq. (B.5) and multiplying $(\cos\varphi - \hat{p}\sin\varphi)$ on both sides leads to

$$\left\{C_{IjKl}\Omega_{1j}\Omega_{1l} + \hat{p}(C_{IjKl}\Omega_{1j}\Omega_{2l} + C_{IjKl}\Omega_{2j}\Omega_{1l}) + \hat{p}^2 C_{IjKl}\Omega_{2j}\Omega_{2l}\right\}a_K = 0. \tag{33}$$

On the other hand, in local coordinates the quadratic eigenvalue problem has the same form compared to Eq. (B.5), i.e.

$$\left\{\hat{C}_{I1K1} + \hat{p}(\hat{C}_{I1K2} + \hat{C}_{I2K1}) + \hat{p}^2\hat{C}_{I2K2}\right\}\hat{a}_K = 0. \tag{34}$$

Considering Eq. (26), Eq. (34) is given by

$$\begin{aligned}\big\{C_{MnPq}\Omega_{1n}\Omega_{1q} + \hat{p}(C_{MnPq}\Omega_{1n}\Omega_{2q} + C_{MnPq}\Omega_{2n}\Omega_{1q}) \\ + \hat{p}^2 C_{MnPq}\Omega_{2n}\Omega_{2q}\big\}\Omega_{IM}\Omega_{KP}\hat{a}_K = 0.\end{aligned} \tag{35}$$

Comparing the two eigenvalue problems according to Eqs. (33) and (35), it is obvious that the terms in braces are identical and they will provide the same eigenvalues $\hat{p}_N$. It is noted that outside the braces, Ω_{IM} doesn't have any associated index with $\Omega_{KP}\hat{a}_K$ and is not a singular matrix. Thus, Ω_{IM} can be eliminated providing

$$a_P = \Omega_{KP}\hat{a}_K \quad \text{or} \quad \hat{a}_K = \Omega_{KP}a_P, \tag{36}$$

and

$$A_{IK} = \Omega_{JI}\hat{A}_{JK} \quad \text{or} \quad \hat{A}_{IK} = \Omega_{IJ}A_{JK}. \tag{37}$$

Having a look at Eq. (B.18), the mathematical rules which govern a_I and A_{IJ} also apply to b_I and B_{IJ}, i.e.

$$\hat{b}_I = \Omega_{IJ}b_J \quad \text{and} \quad \hat{B}_{IK} = \Omega_{IJ}B_{JK}. \tag{38}$$

Eqs. (37) and (38) in connection with the relation for the eigenvalues Eq. (32) enable the transformation of the near-tip solutions Eq. (10).

Next, the Irwin matrix and the material matrix S_{IJ} from Eqs. (13) and (14), being of essential significance for the calculation of fracture mechanical loading quantities, see Eqs. (12) and (21), are transformed. The Irwin matrix in local coordinates is

$$\begin{aligned}\hat{Y}_{IK} &= \Re\Big\{\hat{A}_{IJ}\hat{B}^{-1}_{JK}i\Big\} \\ &= \Re\Big\{\Omega_{IM}A_{MJ}(\Omega_{JN}B_{NK})^{-1}i\Big\} \\ &= \Omega_{IM}\Re\Big\{A_{MJ}B^{-1}_{JN}i\Big\}\Omega_{KN} \\ &= \Omega_{IM}\Omega_{KN}Y_{MN}.\end{aligned} \tag{39}$$

The Irwin matrix is thus transformed just as a second order tensor. The matrix S_{IK} according to Eq. (14), on the other hand, is transformed in this way:

$$\begin{aligned}\hat{S}_{IK} &= \Re\Big\{\hat{B}^{-1}_{IJ}\,\hat{P}^{\mathrm{S1}}_{JL}(\theta=0)\hat{B}_{LK}\Big\} \\ &= \Re\Big\{\Omega_{JM}B^{-1}_{IM}\hat{P}^{\mathrm{S1}}_{JL}(\theta=0)B_{NK}\Omega_{LN}\Big\},\end{aligned} \tag{40}$$

where

$$\hat{P}^{\mathrm{S1}}_{JL}(\theta=0) = \mathrm{diag}(\hat{p}_N). \tag{41}$$

4. Finite element implementation

4.1. Solution of the quasicrystalline boundary value problem

In order to solve the boundary value problem by applying the finite element method (FEM), the weak formulation of QCs is required. For static problems, the variational principle of virtual work is formulated as

$$\delta W - \delta U = 0, \tag{42}$$

where δW is the virtual work from external loading, and U is the intrinsic energy. The energy density according to Eq. (3) can be reformulated as

$$\Phi = \frac{1}{2}\sigma_{ij}\epsilon_{ij} + \frac{1}{2}H_{ij}w_{ij}, \tag{43}$$

and the specific virtual work in QCs is defined as

$$\delta w = t_i \delta u_i + h_i \delta W_i. \tag{44}$$

Hence, the weak formulation is obtained from Eq. (42) by integration of Eqs. (43) and (44):

$$\int_\Gamma \bar{t}_i \delta u_i d\Gamma + \int_\Gamma \bar{h}_i \delta W_i d\Gamma - \frac{1}{2}\delta \int_V (\sigma_{ij}\epsilon_{ij} + H_{ij}w_{ij})\,\mathrm{d}V = 0, \tag{45}$$

where the bar on tractions indicates the loading at the boundary. For setting up algebraic systems of equations and element matrices, the most general technique is the application of isoparametric finite elements [36]. Substituting the constitutive equations Eq. (5) into Eq. (45)

$$\begin{aligned}\int_V \{(C_{ijkl}u_{k,l} + R_{ijkl}W_{k,l})\delta u_{i,j} + (R_{klij}u_{k,l} + K_{ijkl}W_{k,l})\delta W_{i,j}\}\,\mathrm{d}V \\ - \int_\Gamma \bar{t}_i \delta u_i d\Gamma - \int_\Gamma \bar{h}_i \delta W_i d\Gamma = 0,\end{aligned} \tag{46}$$

the displacements in each element can be approximated by interpolation with a sum of shape functions h^α

$$\begin{aligned} u_k &= \sum_{\alpha=1}^{n} h^\alpha \tilde{u}_k^\alpha, \\ W_k &= \sum_{\alpha=1}^{n} h^\alpha \tilde{W}_k^\alpha, \end{aligned} \tag{47}$$

where the displacements with a tilde are the nodal displacements of an element and n is the number of nodes per element. For a quadratic element type, $n = 8$. Inserting these expressions into Eq. (46) yields an approximation of the weak formulation:

$$\begin{aligned}\sum_{\beta=1}^{n} \delta\tilde{u}_i^\beta \left\{ \int_V C_{ijkl} \sum_{\alpha=1}^{n} \frac{\partial h^\alpha}{\partial x_l} \frac{\partial h^\beta}{\partial x_j} \mathrm{d}V \tilde{u}_k^\alpha + \int_V R_{ijkl} \sum_{\alpha=1}^{n} \frac{\partial h^\alpha}{\partial x_l} \frac{\partial h^\beta}{\partial x_j} \mathrm{d}V \tilde{W}_k^\alpha \right\} \\ + \sum_{\beta=1}^{n} \delta\tilde{W}_i^\beta \left\{ \int_V R_{klij} \sum_{\alpha=1}^{n} \frac{\partial h^\alpha}{\partial x_l} \frac{\partial h^\beta}{\partial x_j} \mathrm{d}V \tilde{u}_k^\alpha + \int_V K_{ijkl} \sum_{\alpha=1}^{n} \frac{\partial h^\alpha}{\partial x_l} \frac{\partial h^\beta}{\partial x_j} \mathrm{d}V \tilde{W}_k^\alpha) \right\} \\ - \sum_{\beta=1}^{n} \delta\tilde{u}_i^\beta \int_\Gamma \bar{t}_i h^\beta \, \mathrm{d}\Gamma - \sum_{\beta=1}^{n} \delta\tilde{W}_i^\beta \int_\Gamma \bar{h}_i h^\beta \, \mathrm{d}\Gamma = 0.\end{aligned} \tag{48}$$

By eliminating the virtual displacements $\delta\tilde{u}_i^\beta$ and $\delta\tilde{W}_i^\beta$ due to their independence, Eq. (48) turns into two equations, which are written in matrix form as

$$\begin{aligned}\int_V \underline{B}_u^{\mathrm{T}} \underline{C} \, \underline{B}_u \mathrm{d}V \underline{\tilde{u}} + \int_V \underline{B}_u^{\mathrm{T}} \underline{R} \, \underline{B}_w \mathrm{d}V \underline{\tilde{W}} - \int_\Gamma \underline{N}_u^{\mathrm{T}} \{\bar{t}\} \, \mathrm{d}\Gamma = 0, \\ \int_V \underline{B}_w^{\mathrm{T}} \underline{R}^{\mathrm{T}} \, \underline{B}_u \mathrm{d}V \underline{\tilde{u}} + \int_V \underline{B}_w^{\mathrm{T}} \underline{K} \, \underline{B}_w \mathrm{d}V \underline{\tilde{W}} - \int_\Gamma \underline{N}_w^{\mathrm{T}} \{\bar{h}\} \, \mathrm{d}\Gamma = 0,\end{aligned} \tag{49}$$

where $\underline{B}_u$ and $\underline{B}_w$ are differentiated shape functions for the phonon and the phason displacements at each element and the material coefficients are collected in $\underline{C}$, $\underline{R}$ and $\underline{K}$. $\underline{N}_u$ and $\underline{N}_w$ are the shape function matrices, $\underline{\tilde{u}}$ and $\underline{\tilde{W}}$ are displacement column matrices, comprising the phonon and phason displacement coordinates of all nodes in an element. The dimensions of these matrices depend on n and the number of the phason degrees of freedom. In this part, the index notation is temporarily abandoned for the sake of more compact expressions. The total positive definite stiffness matrix $\underline{K}$ is assembled by different parts

$$\underline{K} = \begin{pmatrix} \underline{K}_{uu} & \underline{K}_{uw} \\ \underline{K}_{uw}^{\mathrm{T}} & \underline{K}_{ww} \end{pmatrix}, \tag{50}$$

where

$$\underline{K}_{uu} = \int_V \left\{ \underline{B}_u^{\mathrm{T}} \underline{C}\, \underline{B}_u \right\} \mathrm{d}V,$$
$$\underline{K}_{uw} = \int_V \left\{ \underline{B}_u^{\mathrm{T}} \underline{C}\, \underline{B}_w \right\} \mathrm{d}V, \tag{51}$$
$$\underline{K}_{ww} = \int_V \left\{ \underline{B}_w^{\mathrm{T}} \underline{C}\, \underline{B}_w \right\} \mathrm{d}V,$$

whereupon the algebraic system of equations finally reads:

$$\underline{K}\, \underline{\tilde{U}} = \underline{F}, \tag{52}$$

with $\underline{\tilde{U}} = (\underline{\tilde{u}}, \underline{\tilde{W}})^{\mathrm{T}}$ and

$$\underline{F} = \begin{pmatrix} \int_\Gamma \underline{N}_u^{\mathrm{T}} \{\bar{t}\}\, \mathrm{d}\Gamma \\ \int_\Gamma \underline{N}_w^{\mathrm{T}} \{\bar{h}\}\, \mathrm{d}\Gamma \end{pmatrix}. \tag{53}$$

The numerical approximation of the integrals Eqs. (51) and (53) is achieved by Gauss quadrature. The above described discretization scheme for QCs has been implemented into the commercial FE software Abaqus as a USER subroutine.

4.2. Crack tip loading analysis and crack path prediction

Based on the numerical calculation of fields according to Sec. 4.1, post processing tools provide the fracture mechanical loading quantities. Crack growth is simulated with an intelligent adaptive re-meshing algorithm [33], whereupon the crack is incrementally extended according to the deflection criterion in Sec. 3.2.

4.2.1. Crack tip element method (CTEM)

The conflict between the validity of near-tip solution and the singularity just in the near-tip field reduces the accuracy of numerical results for SIF. An improved element type named crack tip element meets all requirements of a satisfactory solution quality [29]. This element type constitutes the partition defined by a circular line around the crack tip, see Fig. 4. The elements are degenerated from quadrilateral elements to triangle elements,

where three nodes on a side collapse to one point. In such crack tip elements, the middle nodes at element edges are shifted to quarter point positions into the direction of the crack tip. In this way, the isoparametric elements represent the square root singularity at the crack tip in their shape functions, corresponding to the analytical solution in Eq. (10). The crack opening dis-

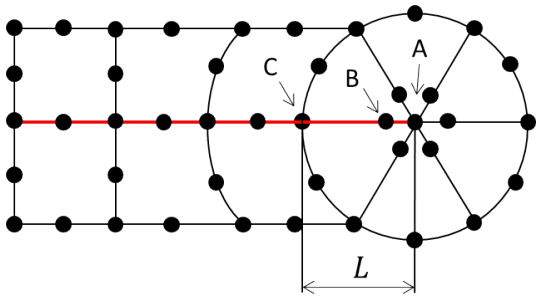

Figure 4: The mesh near the crack tip. Node A at the crack tip, node B is at a quarter position. The nodes on the middle line in red (crack faces) are overlapped double nodes. L is the length between nodes A and C.

placements from Eq. (10) are taken for computing the SIFs. By eliminating $\sqrt{r}$, the SIFs are obtained as

$$K_N = \sqrt{\frac{\pi}{2L}} Y_{NJ}^{-1} (4u_J^B - u_J^C), \tag{54}$$

where u_J^B and u_J^C are displacements at the nodes B and C, see Fig. 4.

4.2.2. J-integral

The J-integral is calculated along an arbitrary contour along element edges and the crack faces, enclosing the crack tip, see Fig. 5. The contour is generated automatically for each step of incremental crack growth. Considering the Eq. (19), the generalized Eshelby tensor Q_{kj} is integrated along the outer path Γ_a and the crack surface integral along Γ^+, Γ^- has to be taken into account. Specifically, J_k is implemented as

$$J_k = \int_{\Gamma_a} (\Phi n_k - t_i u_{i,k} - h_i W_{i,k}) \mathrm{d}\Gamma + \int_{\Gamma^+ + \Gamma^-} \Phi n_k \mathrm{d}\Gamma. \tag{55}$$

For straight cracks, as depicted in Fig. 5, the crack surface integral is not required for the calculation of J_1.

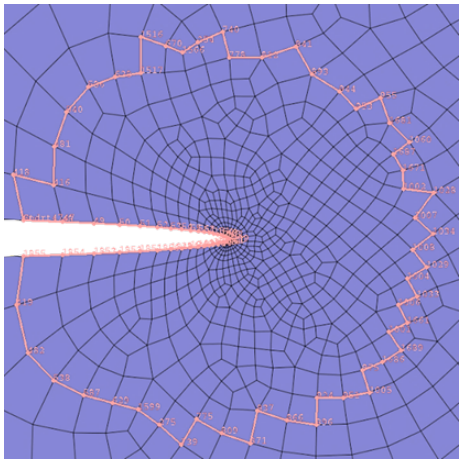

Figure 5: An integral path for computing J_k

5. Numerical results

Although since the discovery of QCs, physicists and chemists have made great progress in diverse fields in QCs, e.g. chemical synthesis on the macroscopic level or measurement of physical properties, it is still difficult to measure the effects pertaining to the phason field. By this means, the coupling constants cited from [37] are more or less hypothetical values, since there isn't any experimental evidence for their correctness. By adopting such constants ($R_1/C_{1111} = 0.47\%$) in previous work [26], it was noticed that the selected QC shows a very weak coupling effect. Moreover, only small phason SIFs could be induced at the crack tip by mechanical loading because phason loading cannot be applied physically. However, the crack paths of classic materials e.g. in [33] show that even a tiny $K_{II}^{\parallel}$ in a $K_I^{\parallel}$-dominated mixed-mode loading, although having little impact on the onset of crack growth, influences crack deflection decidedly. Hence, the influence of phonon-phason coupling on crack paths is investigated, employing specimens or models typically used for the validation of crack path predictions. Since values of coupling constants are not reliable, those of [37] are adopted as reference values, as well as 50 times ($R_1/C_{1111} = 23\%$) and 80 times ($R_1/C_{1111} = 37\%$) enlarged ones.

Obviously, cracks under symmetric Mode-I loading will grow straightforward ($H = -J_2 = 0$). A crack inclined by 30° with respect to the x_1-axis is investigated first, where σ_{22}^{∞} is applied as loading, see Fig 6. $K_{II}^{\parallel}$ is thus on the same level as $K_I^{\parallel}$. Three different coupling constants are presumed

where R^{ref} is the reference value [37]. Crack tip loading is calculated both from the CTEM (Sec. 4.2.1) and the J-integral (Sec. 4.2.2), where G and H are determined applying Eq. (12).

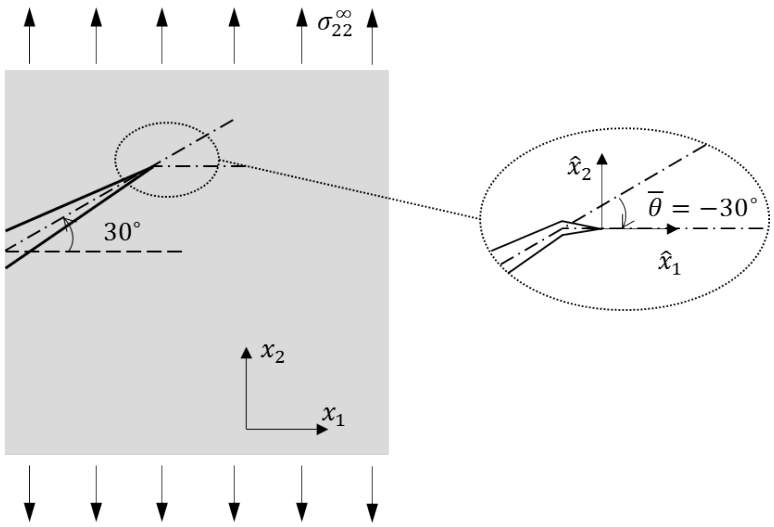

Figure 6: Crack inclined by 30° with respect to the x_1-axis. A kink of -30° is illustrated in detailed view.

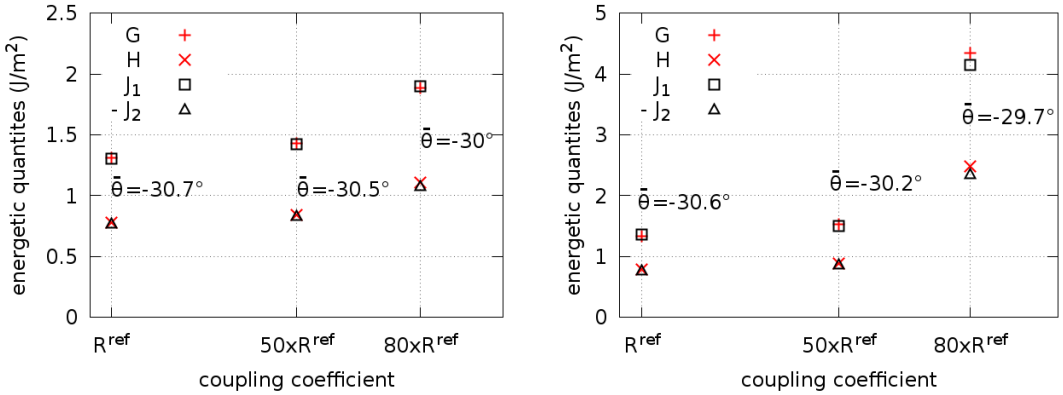

Figure 7: Results of the CTEM (G, H) and the J-integral in a local crack tip coordinate system $(\hat{x}_1, \hat{x}_2)$, as well as crack deflections $\bar{\theta}$ for different coupling constants based on the J-integral criterion; a) QA parallel to the x_1-axis, b) QA parallel to the x_2-axis.

Table 1: Results of the CTEM(G,H) and the J-integral as well as crack deflections $\bar{\theta}$ corresponding to Fig. 7.

	G	H	$\bar{\theta}$	J_1	J_2	$\bar{\theta}$
QA parallel to the x_1-axis						
R^{ref}	1.31	0.78	-30.7°	1.31	-0.77	-30.7°
$50 \times R^{ref}$	1.43	0.84	-30.5°	1.43	-0.84	-30.5°
$80 \times R^{ref}$	1.89	1.10	-30°	1.89	-1.09	-29.8°
QA parallel to the x_2-axis						
R^{ref}	1.33	0.78	-30.6°	1.36	-0.78	-29.8°
$50 \times R^{ref}$	1.52	0.89	-30.2°	1.50	-0.87	-30.1°
$80 \times R^{ref}$	4.34	2.48	-29.7°	4.15	-2.35	-29.5°

The results are shown in Tab. 1 and are also illustrated in Fig. 7 for the sake of clarity. The values $\bar{\theta}$ in the last column of Tab. 1 have been calculated from J_1 and J_2, while the values in the third column stem from G and H, however still based on the J-integral criterion. Two cases are considered, one with the QA in x_1-direction, the other with a perpendicular QA. First of all, G and J_1 and H and $-J_2$, respectively, according to Eq. (20) show almost the same values. Secondly, due to the phason field and its influence on the free energy the loading quantities are increased by enlarged coupling constants. Nevertheless, the crack deflection angles are similar in these three situations, in the case of a QA in x_1-direction and calculation from G and H ranging between $\bar{\theta} = -30.7°$ and $-30°$. The latter value indicates a crack extension perpendicular to the loading direction, see Fig. 6, while the smaller coupling coefficient yields a slight deviation from the x_1-axis. In fact, these small differences have a large impact on the whole crack path, see Figs. 9 and 10. According to the foregoing discussion, small $K_{II}^{\parallel}$ have great effect on the crack growth direction. It could thus be expected that small induced phason SIF may also have a strong influence on the crack path at mixed-mode loading, where $K_I^{\parallel}$ is much larger than $K_{II}^{\parallel}$ and $K^{\perp}$.

In order to establish the desired mixed-mode loading, some typical problems of numerical fracture mechanics are modeled, see Fig. 8. Asymmetric concentrated forces on a double cantilever beam (DCB) specimen, or a hole located on one side of the crack with external tensile loading induce mixed-mode conditions at the crack tip, whereupon $K_{II}^{\parallel}$ and $K^{\perp}$ are relatively small. Two quasiperiodic in-plane directions are considered. One is the QA parallel to the x_1-axis and the other parallel to the x_2-axis, with the incipient crack always being perpendicular to the x_2-direction. The crack paths are plotted in Figs. 9 and 10. Both CTEM and the J-integral have been

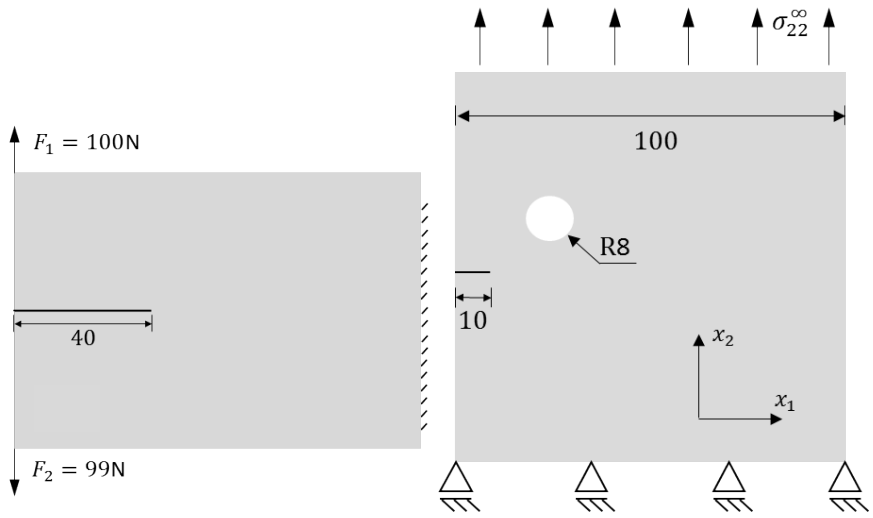

Figure 8: a) DCB model with asymmetric loading, b) plate with a hole above the ligament under tensile loading. The QA is either in the x_1- or the x_2-direction.

applied, see Sec. 4.2, to calculate crack tip loading. The resulting crack paths do not visibly differ from each other.

The solid red lines show the result of $R = R^{\text{ref}}$. The result of $R = 0$ is omitted since the paths are almost overlapping. The dashed green lines, where the coupling constants are 50 times enlarged, are distinctly different from the solid red lines. The dash-dotted blue lines exhibit 80 times the reference values.

Similar to regular crystalline materials [33], the influence of the small $K_{II}^{\parallel}$ in such mixed-mode loading cases emerges in both simulations. For the QA being in x_1-direction, the coupling effect doesn't bring significant changes in the crack paths. When the QA is in x_2-direction, the strong coupling effect essentially compensates the impact of the shear or mode II effect showing the tendency that the crack grows in its original direction in both models. This effect, however, is strongly nonlinear with respect to the coupling constants.

6. Conclusions

In this work, a numerical FE framework has been developed for the solution of boundary value problems of quasicrystals, which introduce a

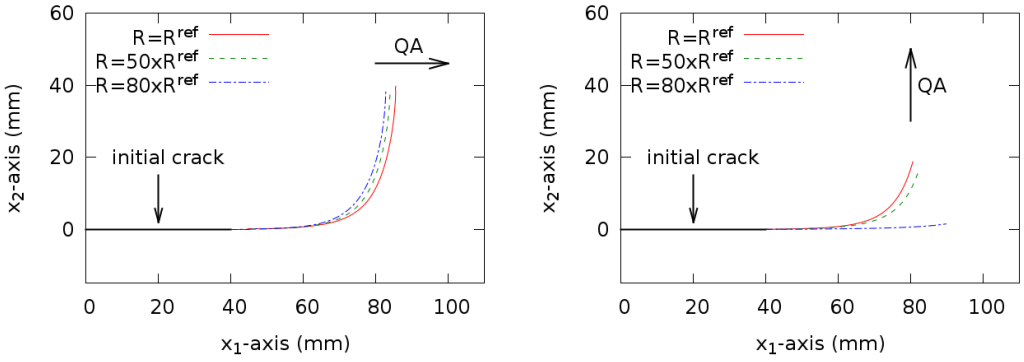

(a) (b)

Figure 9: Results of simulation for DCB model with the QA being a) parallel to the x_1-axis and b) parallel to the x_2-axis.

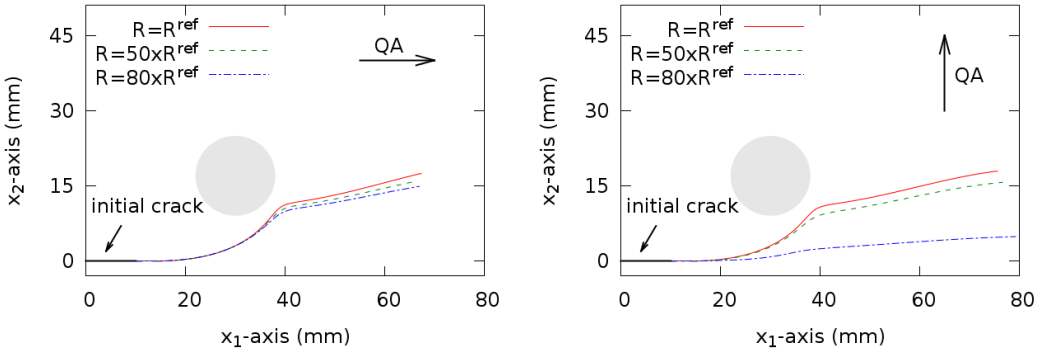

(a) (b)

Figure 10: Results of simulation for plate under tensile loading with a hole and the QA being a) parallel to the x_1-axis and b) parallel to the x_2-axis. The gray circle represents the hole symbolically.

new degree of freedom – the phason field. In order to apply this numerical tool to crack path prediction, the crack tip element method and the J-integral have been implemented. By using the J-integral criterion at mixed-mode loading, the crack deflection angle is determined. An adaptive re-meshing algorithm is constructed to simulate the crack path. Analytical considerations are required to relate fracture quantities for the multi-field

problem. One important feature connected to crack deflection is the careful transformation of material related matrices which is not straightforward.

The impact of the phason field or the coupling effect, respectively, in different specimens manifest some remarkable features. Firstly, the small phason loading at the crack tip, which is induced by phonon loading through the coupling effect, influences the crack path, where $K_{II}^{\parallel}$ is on the same level as $K^{\perp}$. Secondly, the coupling effect of QCs reduces the crack deflection angle, specifically with the QA being perpendicular to the initial crack. For configurations with the QA being parallel to the crack, deviations are smaller.

The coupling coefficient is a property of QCs, where reliable data are hard to get hold of. Experimental values for 1D QCs are still not available, probably since experiments are difficult to design. The crack path simulations have thus been based on different magnitudes of the phonon-phason coupling. The results of the simulations presented in this paper possibly indicate an experimental set-up, where the coupling coefficient is determined from crack paths in plate or DCB specimens with either a hole or with dissimilar mechanical loading.

Appendix A. Material constants and characteristic matrices

In compressed notation the constitutive equations of a 1D QC with the QA being the x_1-axis are

$$\begin{pmatrix} \sigma_{11} \\ \sigma_{22} \\ \sigma_{12} \\ H_{11} \\ H_{12} \end{pmatrix} = \begin{pmatrix} C_{1111} & C_{1122} & 0 & R_2 & 0 \\ C_{1122} & C_{2222} & 0 & R_1 & 0 \\ 0 & 0 & C_{1212} & 0 & R_3 \\ R_2 & R_1 & 0 & K_1 & 0 \\ 0 & 0 & R_3 & 0 & K_2 \end{pmatrix} \begin{pmatrix} \epsilon_{11} \\ \epsilon_{22} \\ 2\epsilon_{12} \\ w_{11} \\ w_{12} \end{pmatrix}. \tag{A.1}$$

The following material constants have been used for the calculations [38, 39, 37]:

$$\begin{aligned} &C_{1111} = 232.22, \quad C_{1122} = 66.63, \quad C_{2222} = 234.33 \\ &C_{1133} = 66.63, \quad C_{2233} = 57.41, \quad C_{3333} = 234.33, \\ &C_{1212} = 70.19, \quad C_{1313} = 70.19, \quad C_{2323} = 88.46, \\ &R_1 = -1.1, \quad R_2 = 0.2, \quad R_3 = 0.5 \\ &K_1 = 122, \quad K_2 = 24, \end{aligned} \tag{A.2}$$

where the unit is GPa and the values of R_i correspond to the reference values R^{ref} in section 5. The material matrix in Eq. (A.1) comes out to be positive definite, even for the enlarged coupling coefficients. For plane stress conditions, the following transformations are required:

$$\begin{aligned}
&C^s_{1111} = C_{1111} - \frac{C_{1133}C_{1133}}{C_{3333}},\\
&C^s_{1122} = C_{1122} - \frac{C_{2233}C_{1133}}{C_{3333}},\\
&C^s_{2211} = C^s_{1122}, \quad C^s_{2222} = C_{2222} - \frac{C_{2233}C_{2233}}{C_{3333}}\\
&C^s_{1212} = C_{1212},\\
&R^s_1 = R_1 - \frac{C_{2233}R_1}{C_{3333}}, \quad R^s_2 = R_2 - \frac{C_{1133}R_1}{C_{3333}}\\
&R^s_3 = R_3,\\
&K^s_1 = K_1 - \frac{R_1R_1}{C_{3333}}, \quad K^s_2 = K_2.
\end{aligned} \tag{A.3}$$

The superscript s indicates the constants for plane stress conditions.

In the general case, the characteristic matrices are 6×6, where 3 rows/columns are from the phonon and the other 3 from the phason field. However, for a plane 1D QC, only 2 of the phonon and 1 of the phason dimensions are required. So, for the quasiperiodic direction along x_1 and the material data according to (A.2) the following complex 3×3 and 1×3 matrices are calculated applying the methods introduced in [28]:

$$\begin{aligned}
A_{MN} &= \begin{pmatrix} -0.00858494 & 1.13626 & 0.55096i \\ -0.00293218i & 0.539528i & -1.14174 \\ 0.999967 & 0.00337372 & -0.00374684i \end{pmatrix},\\
B_{MN} &= \begin{pmatrix} -0.4371i & 148.1i & -107.7 \\ 0.1939 & -107.2 & -151.3i \\ 54.10i & 1.167i & -0.7029 \end{pmatrix} \times 10^9,\\
p_N &= (2.25472i, 1.38257i, 0.711723i).
\end{aligned} \tag{A.4}$$

For the quasiperiodic direction along x_2 they are

$$
\begin{aligned}
A_{MN} &= \begin{pmatrix} -1.14174 & 0.539528i & -0.00293218i \\ -0.55096i & -1.13626 & 0.00858494 \\ 0.00374684i & -0.00337372 & -0.999967 \end{pmatrix}, \\
B_{MN} &= \begin{pmatrix} -151.3i & -107.1 & 0.1939 \\ 107.7 & -148.1i & 0.4371i \\ 0.7029 & -1.167i & -54.10i \end{pmatrix} \times 10^9, \\
p_N &= (1.40504i, 0.723288i, 0.443514i).
\end{aligned}
\tag{A.5}
$$

The matrices $P^{\mathrm{S1}}_{MN}, P^{\mathrm{S2}}_{MN}, P^{\mathrm{u}}_{MN}$ are diagonal matrices and functions of the polar coordinate angle θ, see Fig. 1:

$$
\begin{aligned}
P^{\mathrm{S1}}_{MN} &= \mathrm{diag}\left(\frac{p_J}{\sqrt{\cos(\theta) + p_J \sin(\theta)}}\right), \\
P^{\mathrm{S2}}_{MN} &= \mathrm{diag}\left(\frac{1}{\sqrt{\cos(\theta) + p_J \sin(\theta)}}\right), \\
P^{\mathrm{u}}_{MN} &= \mathrm{diag}\left(\sqrt{\cos(\theta) + p_J \sin(\theta)}\right).
\end{aligned}
\tag{A.6}
$$

Eq. (10) shows the analytical solutions near the crack tip. Alternatively, the stresses and displacements can be split into parts, introducing angular functions being independent on geometry and loading. In detail, the equations of a 3D QC are given as

$$
\begin{aligned}
\sigma_{Mj} = \frac{1}{\sqrt{2\pi r}} \big(& K^{\parallel}_I f^{\parallel I}_{Mj} + K^{\parallel}_{II} f^{\parallel II}_{Mj} + K^{\parallel}_{III} f^{\parallel III}_{Mj} + K^{\perp}_I f^{\perp I}_{Mj} \\
& + K^{\perp}_{II} f^{\perp II}_{Mj} + K^{\perp}_{III} f^{\perp III}_{Mj} \big),
\end{aligned}
\tag{A.7}
$$

$$
\begin{aligned}
u_M = \sqrt{\frac{2r}{\pi}} \big(& K^{\parallel}_I d^{\parallel I}_M + K^{\parallel}_{II} d^{\parallel II}_M + K^{\parallel}_{III} d^{\parallel III}_M + K^{\perp}_I d^{\perp I}_M \\
& + K^{\perp}_{II} d^{\perp II}_M + K^{\perp}_{III} d^{\perp III}_M \big),
\end{aligned}
\tag{A.8}
$$

where f^J_{Mj} are the angular functions of stresses and d^J_M those of the displacements. For plane problems $j = 1, 2$, so the angular functions are

$$
\begin{aligned}
f^J_{M1} &= -\Re\{B_{MN} P^{\mathrm{S1}}_{NI} B^{-1}_{IJ}\}, \\
f^J_{M2} &= \Re\{B_{MN} P^{\mathrm{S2}}_{NI} B^{-1}_{IJ}]\}, \\
d^J_M &= \Re\{A_{MN} P^{\mathrm{u}}_{NI} B^{-1}_{IJ}]\}.
\end{aligned}
\tag{A.9}
$$

The index J of the angular functions runs from 1 to 6 and denotes the corresponding stress intensity factors.

Appendix B. Stroh formalism

The Stroh formalism [40, 41] offers an elegant solution in many fields of anisotropic elasticity, e.g. crack problems and is outlined for QCs in the following. It starts from the constitutive equations and the static balance of momentum equation without body force

$$\sigma_{Ij} = C_{IjKl}\, u_{K,l}, \tag{B.1}$$

$$C_{IjKl}\, u_{K,lj} = 0. \tag{B.2}$$

C_{IjKl} is the compressed elastic stiffness tensor of 1D QCs. The lowercase index runs from 1 to 2 indicating a plane problem, while the uppercase index runs from 1 to 3 comprising the degrees of freedom from the phonon and the phason fields. The state variables are only related to the coordinates (x_1, x_2). It is assumed that the solution of Eq. (B.2) is

$$u_K = a_K f(z), \qquad z = x_1 + p x_2, \tag{B.3}$$

where f is an arbitrary holomorphic function of z, and p and a_K are unknown quantities to be determined. Inserting Eq. (B.3) into Eq. (B.2) yields

$$C_{IjKl}(\delta_{l1} + p\,\delta_{l2})(\delta_{j1} + p\,\delta_{j2}) a_K f''(z) = 0, \tag{B.4}$$

where δ_{ij} is the Kronecker symbol or identity tensor, respectively, and a prime denotes a derivative with respect to z. Since f and z are arbitrary, in general $f''(z)$ is nonzero and can be eliminated to obtain

$$\{C_{I1K1} + (C_{I1K2} + C_{I2K1})p + C_{I2K2}\, p^2\} a_K = 0, \tag{B.5}$$

where the three coefficients of the polynomial $C_{I1K2} + C_{I2K1}$, C_{I1K1} and C_{I2K2} are three 3×3 matrices and the latter two are symmetric and positive definite.

Inherently, Eq. (B.5) is a quadratic eigenvalues problem. The determinant of the term in braces is a polynomial of sixth power in p, therefore three pairs of conjugated complex eigenvalues are obtained [42] and the same holds for the eigenvectors a_K. Introducing complex conjugates with a bar, the eigenvalues and -vectors can be displayed as

$$p^{\alpha+3} = \bar{p}^{\alpha}, \qquad a_K^{\alpha+3} = \bar{a}_K^{\alpha} \qquad (\alpha = 1, 2, 3), \tag{B.6}$$

whereupon the p_N in Appendix A correspond to the p^1, p^2, p^3. The general solution of displacements u_I according to Eq. (B.3) is transformed as:

$$u_K = \sum_{\alpha=1}^{3} \{a_K^{\alpha} f^{\alpha}(z^{\alpha}) + \bar{a}_K^{\alpha} \bar{f}^{\alpha}(\bar{z}^{\alpha})\}. \tag{B.7}$$

Establishing

$$A_{IJ} = a_I^{\alpha=J} \quad \text{and} \quad f_J(z_J) = f^{\alpha=J}(z^{\alpha=J}) \tag{B.8}$$

as a matrix and a vector, the general form of the displacement field in a plane problem is obtained as

$$u_I = A_{IJ} f_J(z_J) + \overline{A}_{IJ} \overline{f}_J(\overline{z}_J). \tag{B.9}$$

Inserting the displacements into Eq. (B.1), the stresses are obtained as

$$\sigma_{Ij} = (C_{IjK1} + p\, C_{IjK2}) a_K f'(z), \tag{B.10}$$

and the separate stress components are

$$\begin{aligned} \sigma_{I1} &= (C_{I1K1} + p\, C_{I1K2})\, a_K f'(z), \\ \sigma_{I2} &= (C_{I2K1} + p\, C_{I2K2})\, a_K f'(z). \end{aligned} \tag{B.11}$$

An additional vector is introduced as

$$b_I = (C_{I2K1} + p\, C_{I2K2})\, a_K = -\frac{1}{p}(C_{I1K1} + p\, C_{I1K2})\, a_K, \tag{B.12}$$

whereupon the second identity is derived from Eq. (B.5). The stress components can be represented as partial differentials of $\phi_I = b_I f(z)$ as follows

$$\begin{aligned} \sigma_{I1} &= -\frac{\partial b_I f(z)}{\partial x_2} = -\frac{\partial \phi_I}{\partial x_2}, \\ \sigma_{I2} &= \frac{\partial b_I f(z)}{\partial x_1} = \frac{\partial \phi_I}{\partial x_1}, \end{aligned} \tag{B.13}$$

where ϕ_I is a stress function vector. Similar to the displacements the matrix B_{IJ} is constructed as

$$B_{IJ} = b_I^{\alpha=J}, \tag{B.14}$$

so that the stress function vector is finally given as

$$\phi_I = B_{IJ} f_J(z_J) + \bar{B}_{IJ} \overline{f}_J(\overline{z}_J). \tag{B.15}$$

It should be noted that the eigenvalues p^α and the matrices A_{IJ} and B_{IJ} dependent on the material constants exclusively, thus they are named as characteristic eigenvalues and matrices. Especially, for transversal isotropy with x_3 as the quasicrystalline axis (QA), the characteristic eigenvalues are

multiple values $p^\alpha = i$. Hence, the plane boundary value problem is degenerated being an isotropic one in the x_1-x_2-plane and thus not solvable directly.

By substituting stress functions from Eq. (B.13) into the constitutive equations, the relationship

$$\begin{pmatrix} C_{I1K1} & 0 \\ C_{I2K1} & -\delta_{IK} \end{pmatrix} \begin{pmatrix} u_{K,1} \\ \phi_{K,1} \end{pmatrix} + \begin{pmatrix} C_{I1K2} & \delta_{IK} \\ C_{I2K2} & 0 \end{pmatrix} \begin{pmatrix} u_{K,2} \\ \phi_{K,2} \end{pmatrix} = 0 \tag{B.16}$$

is obtained. From Eqs. (B.3) and (B.15), respectively, the following relations are obtained

$$u_{I,2} = p\, u_{I,1} \quad \text{and} \quad \phi_{I,2} = p\, \phi_{I,1}, \tag{B.17}$$

which allow transforming Eq. (B.16) into a standard eigenvalue problem formulation

$$\begin{aligned} N^1_{IJ}\, a_J + N^2_{IJ}\, b_J &= p\, a_I, \\ N^3_{IJ}\, a_J + N^1_{JI}\, b_J &= p\, b_I, \end{aligned} \tag{B.18}$$

where

$$\begin{aligned} N^1_{IJ} &= -C^{-1}_{I2K2}\, C_{K2J1}, \\ N^2_{IJ} &= C^{-1}_{I2J2}, \\ N^3_{IJ} &= C_{I1K2}\, C^{-1}_{K2L2}\, C_{L2J1} - C_{I1J1}. \end{aligned} \tag{B.19}$$

References

[1] D. Shechtman, I. Blech, D. Gratias, J. Cahn, Metallic phase with long-range orientational order and no translational symmetry, Phys. Rev. Lett. 53 (20) (1984) 1951–1953.

[2] D. Levine, P. Steinhardt, Quasicrystals: A new class of ordered structures, Phys. Rev. Lett. 53 (26) (1984) 2477–2480.

[3] W. Steurer, S. Deloudi, Crystallography of Quasicrystals: Concepts, Methods and Structures, Vol. 126 of Springer series in materials science, Springer-Verlag Berlin Heidelberg, Berlin, Heidelberg, 2009.

[4] J.-B. Suck, M. Schreiber, P. Häussler, Quasicrystals: An Introduction to Structure, Physical Properties and Applications, Vol. 55 of Springer series in materials science, Springer, Berlin, Heidelberg, 2002.

[5] P. Bak, Phenomenological theory of icosahedral incommensurate (quasiperiodic) order in Mn-Al alloys, Phys. Rev. Lett. 54 (14) (1985) 1517–1519.

[6] D. Levine, T. Lubensky, S. Ostlund, S. Ramaswamy, P. Steinhardt, J. Toner, Elasticity and dislocations in pentagonal and icosahedral quasicrystals, Phys. Rev. Lett. 54 (14) (1985) 1520–1523.

[7] D. Ding, W. Yang, C. Hu, R. Wang, Generalized elasticity theory of quasicrystals, Phys. Rev. B 48 (10) (1993) 7003–7010.

[8] T. Janssen, Crystallography of quasi-crystals, Acta Crystallogr. A 42 (4) (1986) 261–271.

[9] S. Takeuchi, Physical properties of quasicrystals - an experimental review, Mater. Sci. Forum 150-151 (1994) 35–52.

[10] M. Cardona, P. Fulde, K. von Klitzing, R. Merlin, H.-J. Queisser, H. Störmer, Z. M. Stadnik (Eds.), Physical Properties of Quasicrystals, Springer Series in Solid-State Sciences, Springer Berlin Heidelberg, Berlin, Heidelberg, 1999.

[11] U. Koschella, F. Gähler, J. Roth, H.-R. Trebin, Phason elastic constants of a binary tiling quasicrystal, J. Alloy Compd. 342 (1-2) (2002) 287–290.

[12] Y. K. Vekilov, M. A. Chernikov, Quasicrystals, Physics-Uspekhi 53 (6) (2010) 537–560.

[13] A. I. Goldman, Magnetism in icosahedral quasicrystals: current status and open questions, Science and Technology of Advanced Materials 15 (4) (2014) 044801.

[14] J.-M. Dubois, So useful, those quasicrystals, Isr. J. Chem. 51 (11-12) (2011) 1168–1175.

[15] W. Shi, Collinear periodic cracks and/or rigid line inclusions of antiplane sliding mode in one-dimensional hexagonal quasicrystal, Appl. Math. Comput. 215 (3) (2009) 1062–1067.

[16] Y. Gao, A. Ricoeur, Three-dimensional analysis of a spheroidal inclusion in a two-dimensional quasicrystal body, Philos. Mag. 92 (34) (2012) 4334–4353.

[17] X. Wang, P. Schiavone, Dislocations, imperfect interfaces and interface cracks in anisotropic elasticity for quasicrystals, Mathematics and Mechanics of Complex Systems 1 (1) (2013) 1–17.

[18] E. Pan, Some new three-dimensional Green's functions in anisotropic piezoelectric bimaterials, Electronic Journal of Boundary Elements 1 (2) (2003) 236–269.

[19] Y. Gao, A. Ricoeur, Three-dimensional Green's functions for two-dimensional quasi-crystal bimaterials, P. Roy. Soc. A-Math. Phy. 467 (2011) 2622–2642.

[20] X. Li, T. Fan, Y. Sun, A decagonal quasicrystal with a Griffith crack, Philos. Mag. A 79 (8) (1999) 1943–1952.

[21] Y. Gao, A. Ricoeur, L. Zhang, Plane problems of cubic quasicrystal media with an elliptic hole or a crack, Phys. Lett. A 375 (28-29) (2011) 2775–2781.

[22] L.-Z. Yang, A. Ricoeur, F.-M. He, Y. Gao, Finite size specimens with cracks of icosahedral Al–Pd–Mn quasicrystals, Chinese Phys. B 23 (5) (2014) 056102.

[23] J. Sladek, V. Sladek, S. N. Atluri, Path-independent integral in fracture mechanics of quasicrystals, Eng. Fract. Mech. 140 (2015) 61–71.

[24] J. Sladek, V. Sladek, S. Krahulec, C. Zhang, M. Wünsche, Crack analysis in decagonal quasicrystals by the MLPG, Int. J. Fract. 181 (2013) 115–126.

[25] R. Mikulla, J. Stadler, F. Krul, H.-R. Trebin, P. Gumbsch, Crack propagation in quasicrystals, Phys. Rev. Lett. 81 (15) (1998) 3163–3166.

[26] Z. Wang, J. Scheel, A. Ricoeur, Mixed-mode crack tip loading and crack deflection in 1D quasicrystals, Appl. Phys. A 122 (2016) 1041.

[27] T. Fan, Y. Mai, Elasticity theory, fracture mechanics, and some relevant thermal properties of quasi-crystalline materials, Appl. Mech. Rev. 57 (5) (2004) 325.

[28] Y. Gao, A. Ricoeur, L. Zhang, L. Yang, Crack solutions and weight functions for plane problems in three-dimensional quasicrystals, Arch. Appl. Mech. 84 (8) (2014) 1103–1115.

[29] M. Kuna, Finite Elements in Fracture Mechanics, Vol. 201 of Solid Mechanics and Its Applications, Springer Netherlands, Dordrecht, 2013.

[30] H. Ma, Y. H. Chen, The explicit formulations for the J_k vector in both isotropic and anisotropic cases, Int. J. Fracture 75 (2) (1996) R25–R28.

[31] P. O. Judt, A. Ricoeur, G. Linek, Crack path prediction in rolled aluminum plates with fracture toughness orthotropy and experimental validation, Eng. Fract. Mech. 138 (2015) 33–48.

[32] J. D. Eshelby, The force on an elastic singularity, Philos. T. Roy. Soc. A 244 (877) (1951) 87–112.

[33] P. O. Judt, A. Ricoeur, Accurate loading analyses of curved cracks under mixed-mode conditions applying the J-integral, Int. J. Fracture 182 (1) (2013) 53–66.

[34] M. Z. Wang, Advanced elasticity (in Chinese), Peking Univ. Press, 2002.

[35] T. C. T. Ting, Anisotropic elasticity theory and applications, 1st Edition, Vol. 45 of The Oxford engineering science series, Oxford Univ. Press, 1996.

[36] K.-J. Bathe, Finite element method, in: Wiley Encyclopedia of Computer Science and Engineering, John Wiley & Sons, Inc, 2007.

[37] K. Edagawa, Phonon–phason coupling in decagonal quasicrystals, Philos. Mag. 87 (18-21) (2007) 2789–2798.

[38] M. A. Chernikov, H. R. Ott, A. Bianchi, A. Migliori, T. W. Darling, Elastic moduli of a single quasicrystal of decagonal Al-Ni-Co: Evidence for transverse elastic isotropy, Phys. Rev. Lett. 80 (2) (1998) 321–324.

[39] H.-C. Jeong, P. J. Steinhardt, Finite-temperature elasticity phase transition in decagonal quasicrystals, Phys. Rev. B 48 (13) (1993) 9394–9403.

[40] A. N. Stroh, Dislocations and cracks in anisotropic elasticity, Philos. Mag. 3 (30) (1958) 625–646.

[41] A. N. Stroh, Steady state problems in anisotropic elasticity, J. Math. Phys. Camb. 41 (1-4) (1962) 77–103.

[42] J. D. Eshelby, W. T. Read, W. Shockley, Anisotropic elasticity with applications to dislocation theory, Acta Metall Mater. 1 (3) (1953) 251–259.